Atmospheric Chemistry and Physics

Evolution of organic aerosol mass spectra upon heating: implications for OA phase and partitioning behavior

C. D. Cappa[1] and K. R. Wilson[2]

[1]Department of Civil and Environmental Engineering, University of California, Davis, CA 95616, USA
[2]Chemical Sciences Division, Lawrence Berkeley National Laboratory, Berkeley, CA 94720, USA

Abstract. Vacuum Ultraviolet (VUV) photoionization mass spectrometry has been used to measure the evolution of chemical composition for two distinct organic aerosol types as they are passed through a thermodenuder at different temperatures. The two organic aerosol types considered are primary lubricating oil (LO) aerosol and secondary aerosol from the α-pinene $+ O_3$ reaction (αP). The evolution of the VUV mass spectra for the two aerosol types with temperature are observed to differ dramatically. For LO particles, the spectra exhibit distinct changes with temperature in which the lower m/z peaks, corresponding to compounds with higher vapor pressures, disappear more rapidly than the high m/z peaks. In contrast, the αP aerosol spectrum is essentially unchanged by temperature even though the particles experience significant mass loss due to evaporation. The variations in the LO spectra are found to be quantitatively in agreement with expectations from absorptive partitioning theory whereas the αP spectra suggest that the evaporation of αP derived aerosol appears to not be governed by partitioning theory. We postulate that this difference arises from diffusivity within the αP particles being sufficiently slow that they do not exhibit the expected liquid-like behavior and perhaps exist in a glassy state. To reconcile these observations with decades of aerosol growth measurements, which indicate that OA formation is described by equilibrium partitioning, we present a conceptual model wherein the secondary OA is formed and then rapidly converted from an absorbing form to a non-absorbing form. The results suggest that, although OA growth may be describable by equilibrium partitioning theory, the properties of organic aerosol once formed may differ significantly from the properties determined in the equilibrium framework.

1 Introduction

Atmospheric aerosol particles play an important role in the Earth's climate system through their ability to absorb and scatter solar radiation and influence the properties of clouds (IPCC, 2007) and have significant negative effects on human health (e.g. Pope et al., 2009). Aerosols are comprised of a wide variety of materials, with organic components commonly making up over 50% of the sub-micron aerosol mass (Zhang et al., 2007). Despite the ubiquity of organic aerosol (OA), much remains unknown with respect to formation, chemical evolution and removal mechanisms. Atmospheric models of OA formation generally follow from absorptive partitioning theory (Pankow, 1994), using either a two-product (Odum et al., 1996) or volatility basis-set (Donahue et al., 2006; Robinson et al., 2007) framework. Unfortunately, the use of these approaches in models has typically led to either an under-estimate of ambient OA mass loadings (e.g. Heald et al., 2005; Volkamer et al., 2006) or model OA with physical properties, such as volatility, that are inconsistent with observations (Dzepina et al., 2009). Quantitative estimates of OA volatility for ambient aerosol suggest the presence of components with volatilities that are significantly lower than has been deduced from in-chamber OA growth experiments or could likely be formed from typical gas-phase chemical reactions (Cappa and Jimenez, 2010). These types of observations suggest that there is a gap between our understanding of OA obtained from aerosol growth experiments and measurements of volatility once the aerosol is formed.

Here, we investigate the volatility and evaporation behavior of two distinct aerosol types: lubricating oil (LO) aerosol, a proxy for primary OA, and secondary OA formed from the reaction of α-pinene with O_3 (αP SOA). Based on previous laboratory experiments, it is thought that molecular components of LO and αP aerosol have similar volatility distributions (Presto and Donahue, 2006; Pathak et al., 2007b; Lane et al., 2008; Grieshop et al., 2009). However, we find

evidence that, during evaporation, these two aerosol types exhibit dramatically different evaporation rates and changes to the particle composition, as deduced from vacuum ultraviolet (VUV) aerosol mass spectrometry measurements. The LO aerosol exhibits behavior that is consistent with partitioning theory, whereas the behavior of the αP aerosol is quite different and cannot be explained via traditional partitioning theory. Our results are consistent with the SOA particles having very slow diffusion, perhaps existing in a glassy state, in line with other recent results for SOA (Virtanen et al., 2010; Vaden et al., 2011). To understand these results in the context of aerosol growth experiments, we postulate a conceptual model for SOA formation based on a modified form of absorptive partitioning theory.

2 Methods

2.1 Vacuum Ultraviolet – Aerosol Mass Spectrometer (VUV-AMS)

Mass spectra of organic aerosol were measured using the VUV-AMS located at the Chemical Dynamics Beamline at the Advanced Light Source (Mysak et al., 2005; Shu et al., 2006; Smith et al., 2009). In this VUV-AMS, particles are focused in an aerodynamic lens and introduced into an ionization chamber held at $\sim 10^{-5}$ Torr, where the particles are vaporized on a heated plate. The plate is held at a constant temperature, fixed between 100 and 250 °C. As the particles impact the heated plate they vaporize to produce gas-phase species that are ionized by 10.5 eV photons. The resulting ions are extracted into a time-of-flight mass spectrometer ($m/\Delta m \sim 2000$). Background spectra are collected before and after each aerosol mass spectrum by closing the aerosol inlet. Compared to a conventional electron impact-based AMS, fragmentation of the parent compounds is significantly reduced due both to the use of VUV photons for ionization and the use of a lower heater temperature (see Fig. 1).

2.2 Organic aerosol generation

2.2.1 Lubricating oil aerosol

Lubricating oil (LO) aerosol was generated via homogeneous nucleation by passing clean, dry N_2 over 10W-30 motor oil heated to ~ 80 °C. As the air cools, particles nucleate with a log-normal distribution, typically with a median volume-weighted diameter, $d_{p,V}$, between 220 nm–250 nm and a geometric standard deviation, σ_p, of 1.35–1.4. The aerosol concentration was controlled by passing the particle-laden air stream through a filter-based "diluter." In the diluter, the aerosol flow is split between a 1/8 copper tube and a particle filter, with the exact split controlled using a needle valve located downstream of the filter. Particle number concentrations can be reduced by up to ca. a factor of 10 using the diluter. The aerosol was then passed through a glass flowtube
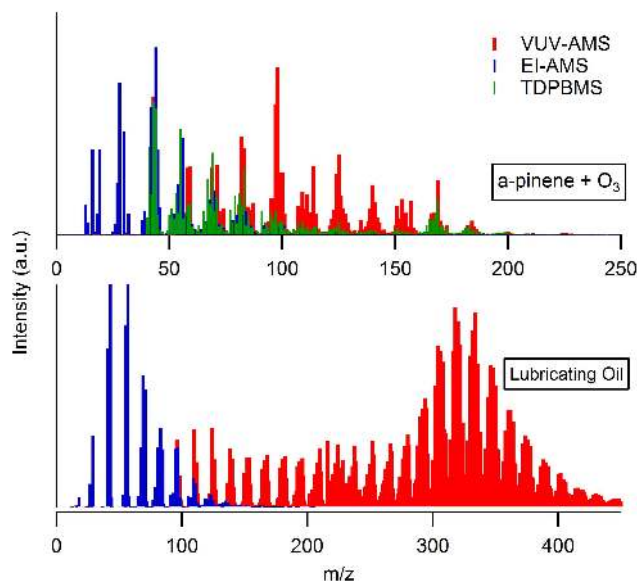

Fig. 1. Mass spectra for primary lubricating oil aerosol (bottom) and SOA from α-pinene + O_3 (top) measured using the VUV-AMS (red), a conventional Aerodyne EI-AMS (blue) and the Ziemann Group EI-AMS (green, αP only). Note the much greater number of high m/z peaks for the VUV mass spectrum compared to the EI mass spectrum. Part of this difference is attributable to the different ionization methods and part to the lower vaporization temperatures employed in the VUV-AMS. EI mass spectra are from (Ulbrich et al., 2009, 2010; Ziemann et al., 2010).

with a 37 s mixing time before finally passing to the thermodenuder (described below). The initial particle mass loading was typically around 650 µg m^{-3}.

2.2.2 Secondary organic aerosol

Secondary organic aerosol was produced from homogeneous nucleation of the products from the reaction of α-pinene and O_3 (referred to as αP aerosol). α-pinene vapor was introduced by continuously injecting a small amount of α-pinene liquid into a 1 lpm flow of dry N_2 and then sub-sampling 0.1 lpm of this flow into the reaction flowtube. O_3 was generated by passing 1 lpm of pure O_2 over an Hg pen-ray lamp and then sub-sampling 0.05 lpm of this O_3 flow into the reaction flowtube. The α-pinene and O_3 were diluted into nitrogen such that the total flow was 1 lpm with N_2:O_2 = 9:1 and were allowed to react in a cylindrical glass flowtube ($L = 1.7$ m; $D = 6.35$ cm), with a total reaction time of ca. 320 s. No OH scavenger was used. Given the short residence time (compared to environmental chamber experiments), it was necessary to use relatively high concentrations of reactants: ~ 13 ppm α-pinene and 1 ppm O_3. The O_3 concentration was measured using an O_3 monitor (2B technologies), whereas the α-pinene concentration was estimated from the syringe pump and gas flow rates. By using excess α-pinene, it was ensured that all of the O_3 reacted in the flowtube. Typical

initial mass loadings for αP aerosol were ca. 500 µg m^{-3} with $d_{p,V} = 92$ nm, $N_p \sim 1.8 \times 10^6$ particles cm^{-3} and $\sigma_p = 1.38$.

2.2.3 Mixed aerosol

In one experiment, αP aerosol was coated onto LO seed particles. This was done by producing LO particles via homogeneous nucleation (with $d_{p,N} = 157$ nm, $\sigma_p = 1.38$) as above and then using these LO particles as seed particles for condensation of the α-pinene + O$_3$ reaction products ($d_{p,N} = 188$ nm, $\sigma_p = 1.42$). The particle number concentration did not increase significantly (by less than 5%), indicating that the majority of the αP aerosol was internally mixed with the LO aerosol. Nucleated αP aerosol was easily identified as a unique mode with $d_{p,N} = 32$ nm and contributed less than 0.2% to the total particle mass, and thus will not influence the VUV-AMS measurements. The mass ratio between LO and αP aerosol in the mixed particles was ca. 2:3, estimated assuming a density for αP aerosol of 1.3 g cm^{-3} (Shilling et al., 2009) and for LO aerosol of 0.88 g cm^{-3}. The total mass loadings were ca. 500 µg m^{-3}.

2.3 Thermodenuder

The thermodenuder (TD) was of the same design as the TD described by (Huffman et al., 2008). The TD consisted of a variable-temperature heated section ($L = 0.5$ m, $D = 2.2$ cm) followed by an activated carbon denuder/cooling section ($L = 0.41$ m, $D = 1.9$ cm). The ambient temperature flowrate through the TD was 0.6 lpm, giving an effective plug flow residence time of $\sim$15 s. Measurements were made with the temperature of the heated section ranging from ambient temperature up to 170 °C. Particle composition and size measurements were made both after passing the particles through a bypass line (at ambient temperature) or through the TD. Bypass measurements were made at every TD temperature in order to account for any changes to the original size distributions (although such changes were negligible during a given experiment).

2.4 Size distributions

Particle size distributions were measured using a scanning mobility particle sizer (SMPS; TSI, Inc.) operating with an aerosol flow of 0.3 lpm and a sheath flow of 3 lpm. The lower and upper size limits in this configuration were 14.3 nm and 673 nm, respectively.

3 Results and discussion

Size distributions and VUV mass spectra were measured for LO, αP and mixed LO/αP aerosol as a function of the TD temperature (T_{TD}). The initial distributions for all aerosol types were log-normal. As T_{TD} increased, the particle mass loading (C_p) and d_p decreased for each aerosol type. Using
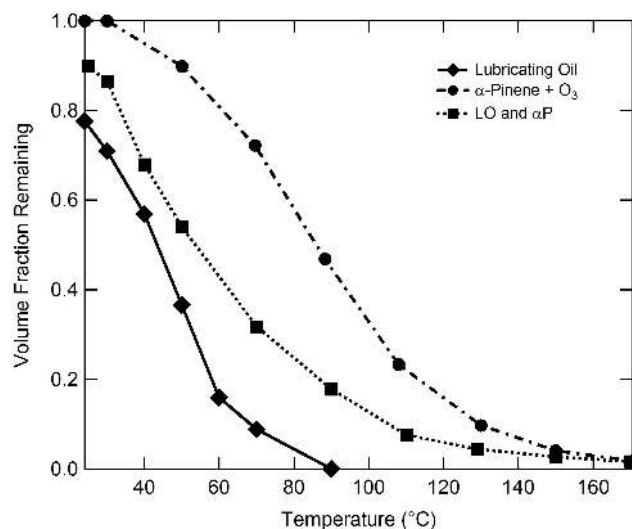

Fig. 2. Mass thermograms for LO aerosol ($\blacklozenge$), αP aerosol ($\bullet$) and the LO/αP mixture ($\blacksquare$). In the mixed particles, the LO is observed to disappear rapidly as temperature is increased while the αP spectrum remains nearly unchanged.

as a reference state the volume-weighted particle diameter, $d_{p,V}$, as measured from the bypass line, the volume fraction remaining (VFR) was determined as a function of T_{TD} (Fig. 2) based on the changes in the particle size. By using particle size changes, we are effectively determining the mass loss due to evaporation alone. For particles of constant density this is equivalent to a mass thermogram. The distribution width, σ_g, only changes slightly from low to high T_{TD}, indicating that preferential loss of small particles is not significantly influencing our results. The decrease in VFR from 1 at a given T_{TD} followed the order LO > LO/αP > αP aerosol (Fig. 2). Since each of these experiments was conducted at a similar mass loading (Saleh et al., 2010), it is possible to conclude that the LO aerosol is somewhat more volatile than αP aerosol, as has previously been deduced from other TD measurements (An et al., 2007; Huffman et al., 2009b). For both LO and mixed LO/αP aerosol at ambient temperature the measured VFR was found to be significantly less than 1 (VFR = 0.78 and 0.9, respectively). The mixed LO/αP mass thermogram can be represented well as a linear combination of the LO and αP mass thermograms.

3.1 VUV mass spectra as a function of T_{TD}

The VUV mass spectra for both LO and αP aerosol contain many more "high" mass peaks compared to the mass spectra obtained using more conventional electron impact AMSs (Fig. 1). This suggests that the VUV spectra can provide more direct information as to the behavior of parent ions than does an EI spectrum. For example, for LO many of the observed peaks are in the range $m/z = 250$–450. This corresponds to compounds with around 18–32 carbon atoms,

peaking around $N_c = 23 - 24$. This is generally consistent with the composition of the source lubricating oil, for which various gas chromatograms of (non-aerosol) 10W-30 LO indicate that the peak carbon number is around 26–27 carbon atoms (Reardon et al., 2007; Lambe et al., 2009). This suggests that our LO aerosol is somewhat more volatile than the source LO, a result consistent with Grieshop et al. (2009) who found that LO aerosol produced from flash vaporization was slightly more volatile than the source LO (smaller N_c by ~1–2 carbon atoms). Our LO aerosol therefore may be comprised of slightly more volatile components than the Grieshop et al. (2009) aerosol due to differences in aerosol generation methods. However, it should be kept in mind that any fragmentation that does occur in the VUV-AMS will tend to skew the observed mass spectrum towards smaller N_c compounds. Thus, the above discussion suggests that the overall differences in LO composition are likely to be relatively small (the importance of this observation will be seen in Sect. 3.2).

For αP aerosol there is significant spectral intensity at $m/z > 136$ (the MW of α-pinene), although fragmentation appears to be somewhat greater in the αP system compared to LO. The observed VUV-MS for αP aerosol is reasonably similar to that obtained by Johnston and co-workers using their photoionization aerosol mass spectrometer (Tolocka et al., 2006; Gao et al., 2010).

The evolution of the VUV aerosol mass spectra for LO, LO/αP and αP aerosol with T_{TD} is shown in Figure 3. To facilitate visual comparison between spectra measured at different T_{TD} (and therefore at different mass loadings), the spectra have been area normalized to a particular m/z or range of m/z. For the LO aerosol, clear m/z dependent changes in the VUV mass spectrum were observed with T_{TD} (Fig. 3). Specifically, the relative intensities of lower m/z (higher volatility) peaks decrease faster with T_{TD} than higher m/z (lower volatility) peaks, and above the normalization range (where the intensity is constant with T_{TD}) the intensity actually increases with T_{TD}. This is shown more explicitly in Fig. 4a, where the spectral intensity of every peak from 250–477 amu, now normalized to the absolute value from the bypass spectrum, is shown as a function of T_{TD}. (This is analogous to a mass thermogram determined from the SMPS measurements and will be termed a "peak thermogram.") Furthermore, the peaks have been binned into groups with $\Delta m/z = 14$ to highlight the m/z dependence (Fig. 4b). The low m/z peaks exhibit the largest decrease in intensity at ambient temperature followed by the fastest decay with T_{TD}. By comparison, the highest m/z peaks exhibit minimal loss in intensity after passing through the TD at ambient temperature with a more gradual loss in peak intensity as a function of increasing T_{TD}. For the hydrocarbon compounds comprising LO aerosol, molecular weight (i.e. m/z) is a reasonable proxy for vapor pressure and thus the preferential loss of the low m/z peaks corresponds to loss of the higher volatility components. In principle, we would then expect a continu-
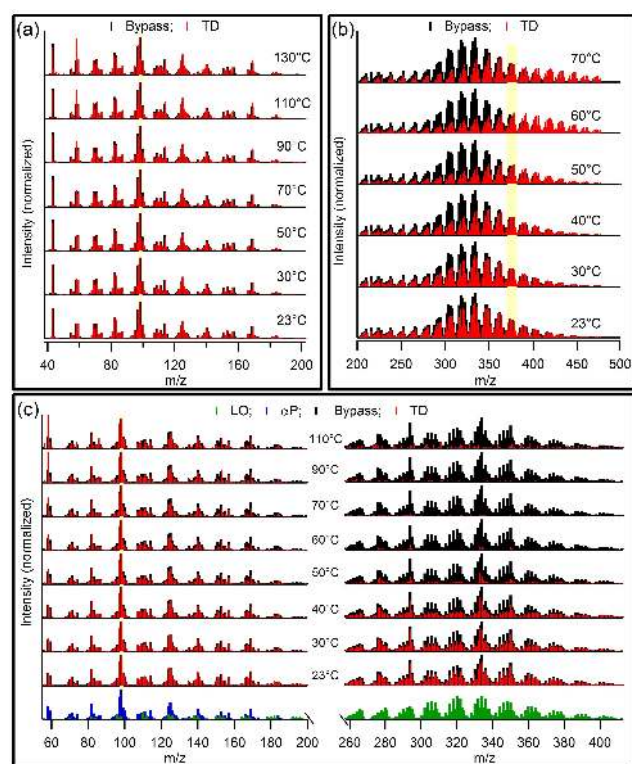

Fig. 3. VUV mass spectra of thermodenuded OA are shown as a function of the thermodenuder temperature (red). The spectra of the particles through the bypass line are shown for reference (black). **(a)** Spectra for αP particles, normalized to the peak at $m/z = 98$. **(b)** Spectra for LO particles, normalized to the range $m/z = 370$–380. **(c)** Spectra for mixed LO + αP particles, normalized to the peak at $m/z = 98$. For reference, spectra for αP aerosol (blue) and LO aerosol (green) are shown individually. Note the break in the x-axis and also that the spectral intensity in the right graph ($m/z = 260$–415) has been multiplied by a factor of 4 relative to the left graph ($m/z = 55$–200).

ous decrease in MFR with MW at a given T_{TD}. However, fragmentation of higher MW species will contribute peaks at lower MW that will exhibit the same thermal behavior as the parent (high MW) peak. As such, the observed "bunching up" of the lower m/z peak thermograms likely results from contributions of fragments from higher m/z compounds, and thus a loss of information as to the evaporation behavior of lower MW species.

The variation in the VUV mass spectrum with T_{TD} for αP aerosol is dramatically different than that observed for LO aerosol. The αP aerosol spectrum is nearly independent of T_{TD}, both for peaks above and below m/z 136 (Fig. 3). This is especially apparent when one considers the peak thermogram for αP aerosol, where nearly every peak exhibits the same dependence on T_{TD} (Fig. 5a). This suggests that, although the total particle mass decreases with increasing T_{TD}, the chemical composition remains nearly independent
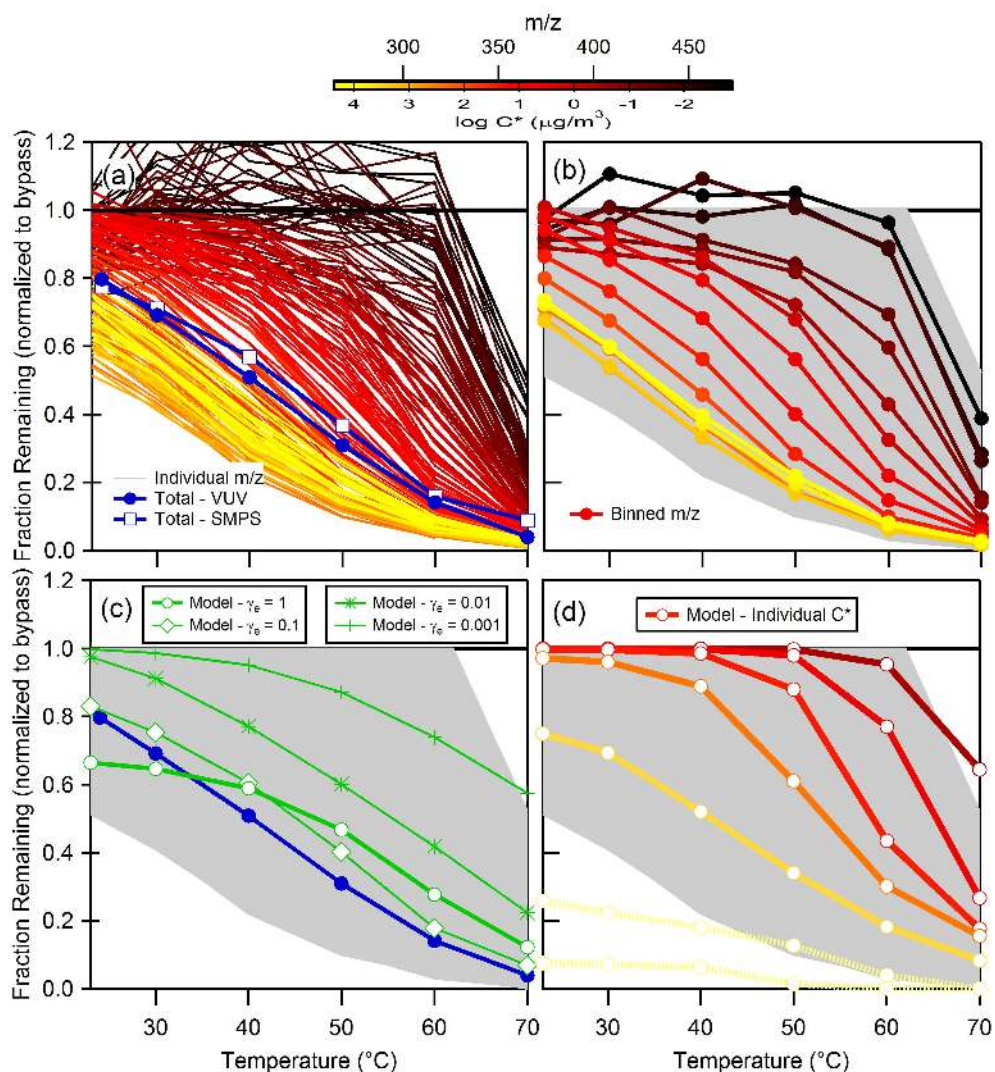
Fig. 4. **(a)** Total mass thermograms (blue) from SMPS (open squares) and VUV intensity (filled circles) measurements and peak thermograms for every *m/z* from *m/z* = 260 to 477 amu (thin lines) for LO particles. Line colors indicate the *m/z* (see color scale). **(b)** Same as **(a)**, but where the results from the individual peaks have been binned into narrower mass ranges to illustrate the *m/z* dependence. **(c)** Calculated total mass thermograms for model LO aerosol for different values of γ_e (green). The measured value is shown for reference (blue). **(d)** Calculated mass thermograms for each model LO component (i.e. different C^*) are shown, assuming $\gamma_e = 0.5$. Line colors correspond to the C^* values and range from 10^{-2} to 10^4 µg m^{-3}. Note that the $C^* = 10^3$ and 10^4 µg m^{-3} components are above the color scale and shown as faded to indicate this. The gray region in panels **(b)**, **(c)** and **(d)** indicates the range over which individual *m/z* peak thermograms in **(a)** were observed.

of temperature. For the αP aerosol we would not necessarily expect any specific MW dependence because the nature of the oxygen-containing functional groups will play an important role in determining the volatility of a given compound. However, just as LO aerosol is comprised of compounds with a wide distribution of vapor pressures (Grieshop et al., 2009), aerosol yield experiments suggest that αP aerosol is similarly composed of compounds with a distribution of vapor pressures (e.g. Griffin et al., 1999; Ng et al., 2006; Presto and Donahue, 2006). Thus, it is very surprising that the VUV mass spectrum for αP aerosol is nearly insensitive to T_{TD},

since we would expect at least some of the peaks to correspond to compounds with different vapor pressures and thus to evaporate at different rates. It is possible that the peaks observed in the VUV mass spectrum are biased towards compounds with specific functional groups, which would complicate the interpretation. However, the observed overall peak thermogram agrees well with the observed SMPS-derived mass thermogram, which suggests that our results are not biased in any particular direction (e.g. more vs. less volatile components, Fig. 5a). (The overall peak thermogram intensity has been corrected for the observed particle number loss

in the thermodenuder relative to the bypass.) These observations indicate that, although αP aerosol is comprised of many different individual compounds (e.g. Yu et al., 1999; Docherty et al., 2005), the overall volatility is governed by some other effective physical parameter and not solely the properties of each individual compound. In other words, it is as if the αP particles were comprised of a single "meta-compound." The exception to the above is the relative behavior of the peak at m/z 58, which increases with T_{TD}. It is not clear why this peak behaves differently than the majority of the spectrum.

The ambient temperature VUV mass spectrum of the mixed LO/αP particles is reasonably well represented as a sum of the pure LO and αP particle spectra. The peaks in the mass spectrum corresponding to LO and αP are well separated such that it is possible to follow their evolution in the mixed system separately. This allows the evolution of the overall mass spectrum of mixed LO/αP particles with T_{TD} to be analyzed as a linear combination of the two individual aerosol spectra. The intensity of the LO peaks decrease relative to the αP peaks with increasing T_{TD} such that once $T_{TD} > 70\,°C$ the spectrum resembles that of pure αP particles. Also, like the pure LO aerosol, there is a clear m/z dependence to the spectral variation with T_{TD} in the LO region of the spectrum. Thus, even though the LO and αP are internally mixed (as evidenced by the lack of increase in particle number concentration), it appears that within a particle the LO and αP components do not mix at a molecular level to a significant extent. Recall that the αP aerosol was coated onto LO seed particles, and thus one might expect that the αP material should form a shell around the LO particles as was previously observed for αP aerosol on dioctyl phthalate particles (Vaden et al., 2010). However, if αP aerosol formed a shell around the LO particles then it is reasonable to expect that the evaporation of the LO core should have been significantly impeded by the αP coating, yet this was not observed. Instead, our results appear consistent with the mixed LO/αP aerosol having a morphology wherein the LO and αP components exist as separate phases in a "side-by-side" arrangement, thus allowing the LO components to evaporate essentially unimpeded by the αP components. This observation is consistent with the mass thermogram for the mixed LO/αP being a linear combination of the individual LO and αP mass thermograms.

3.2 Mass and peak thermograms: quantitative analysis

Mass thermograms for the LO and αP multi-component aerosol particles have been calculated using a kinetic model of aerosol evaporation in the thermodenuder (Cappa, 2010). Implicit to the model is the assumption that the particles are well-mixed and describable through absorptive partitioning theory (i.e. governed by Raoult's Law, perhaps with activity coefficient adjustments). The required inputs to the model are a volatility basis-set of ambient temperature
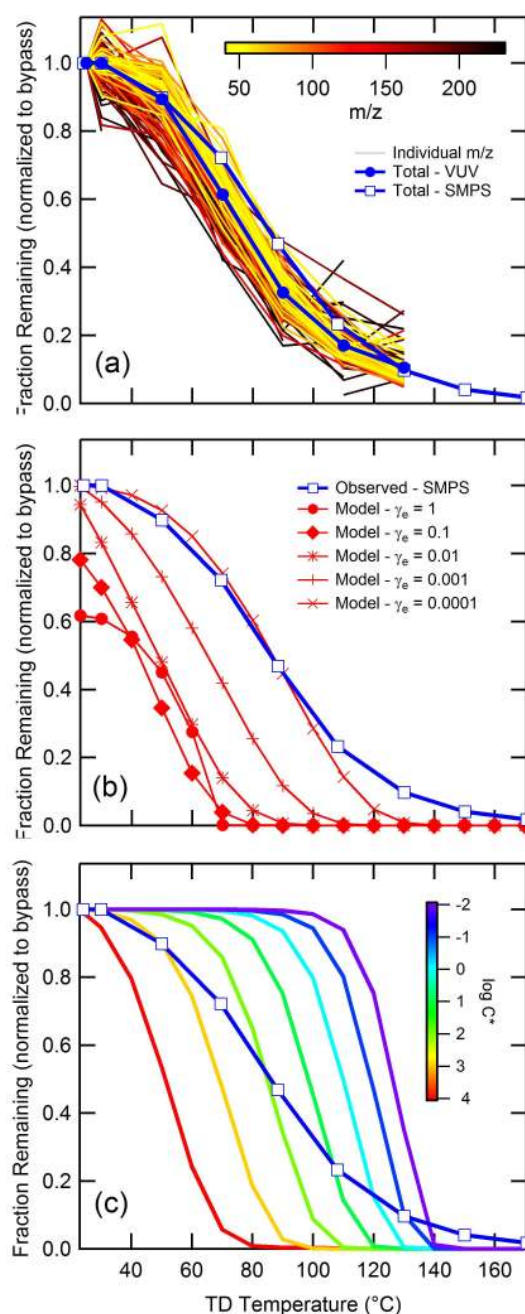

Fig. 5. (a) The measured individual peak thermograms over the range $m/z = 42$–230 are shown (see color scale) along with the average peak (blue ●) thermogram and the SMPS-derived mass thermogram (blue □) for αP particles. **(b)** Calculated mass thermograms for low-NO$_x$ αP aerosol are shown for different assumed γ_{evap} values (see legend). The observed total mass thermogram is shown for reference. **(c)** Calculated thermograms for the individual C^* components assuming that $\gamma_e = 10^{-4}$, indicating that distillation would still be expected. Line colors correspond to component C^* values (see color scale). The observed total mass thermogram is shown for reference.

saturation concentrations (C^*) with the total mass fraction (gas + particle phase) of each component in the basis-set specified (α_i), the total OA mass (C_{OA}), the enthalpy of vaporization (ΔH_{vap}), molecular weight (MW), gas-phase diffusivity (D_g) and evaporation coefficient (γ_e). Here, a logarithmically spaced C^* basis-set has been used. The initial particle phase fraction for each compound is determined from:

$$\xi_{p,i} = \left(1 + \frac{C_i^*}{C_{OA}}\right)^{-1}; C_{OA} = \sum_i C_{OA,i} = \sum_i \xi_{p,i} \alpha_i C_{tot}. \quad (1)$$

where $\xi_{p,i}$ is the partitioning coefficient and α_i is the stoichiometric yield for compound i, and C_{tot} is the total (gas + particle phase) concentration of all compounds (Odum et al., 1996).

For LO aerosol we have used the C^* basis-set for diesel aerosol (thought to be primarily composed of lubricating oil) from Grieshop et al. (2009), where $C^* = \{0.01, 0.1, 1, 10, 100, 1000, 10^4\}\,\mu g\,m^{-3}$ and $\alpha_i = \{0.01, 0.01, 0.04, 0.21, 0.18, 0.45, 0.1\}$. (Grieshop et al. (2009) state that there is a small amount of mass required in a $C^* = 0.001\,\mu g\,m^{-3}$ bin, but that this mass was incorporated into the $0.01\,\mu g\,m^{-3}$ bin. We find that inclusion of a $C^*,= 0.001\,\mu g\,m^{-3}$ bin in our model does not affect our results.) As already discussed, the method of generation of LO aerosol in this study and in the Grieshop et al. (2009) study were different, which may contribute to some differences in the actual LO aerosol composition, potentially making the LO particles here somewhat more volatile than in the study in which the basis-set fit was derived. ΔH_{vap} values were estimated using the relationship given in Epstein et al. (2009). The assumed ΔH_{vap} distribution used here is different than that used by Grieshop et al. (2009) to determine their volatility basis-set fit. We find that this alteration allows for more robust simulation of the shape of the LO mass thermograms. The need for this change likely results from the use of an explicitly kinetic model here (Cappa, 2010) compared with the assumption of equilibrium in the TD in the Grieshop et al. (2009) study. Although this adds some uncertainty to our analysis, it does not change the general conclusions. MW values were specified using an estimated C^*/MW relationship, where log $C^* = -0.0337MW + 11.56$ (Lide, 2005); this relationship is only applicable to saturated hydrocarbons. We assume that the gas-phase diffusion coefficient $D_g = 3 \times 10^{-6}\,m^2\,s^{-1}$ and use $d_p = 240\,nm$ and $C_{OA} = 730\,\mu g\,m^{-3}$ (the observed values) along with the actual physical dimensions of the TD (Huffman et al., 2008; Cappa, 2010). Given the uncertainties in the volatility basis-set and ΔH_{vap} values, the model does a good job of reproducing the observations for the total mass thermogram when the evaporation coefficient, γ_e, value is assumed to be 1 or 0.1 (Fig. 4c). (The reason the $\gamma_e = 1$ and 0.1 cases cross-over in the calculations originates from a balance between evaporation in the heated section and the re-condensation in the ambient temperature denuder section

of the TD at the high mass loadings used in these experiments.) However, when lower values for γ_e are assumed the model/measurement agreement is poor, especially at room temperature. This observation clearly demonstrates that the components comprising the LO aerosol can be considered "semi-volatile." Mass fraction remaining (MFR) values as a function of T_{TD} are also shown for the individual components considered in the model (i.e. the compounds with different C^* values) and show generally good correspondence with the observed binned peak thermograms (where $\gamma_e = 0.5$ has been used for illustration since both $\gamma_e = 1$ and 0.1 yield reasonably good results; see Fig. 4d). Note that if our LO aerosol is actually more volatile than the LO aerosol used to derive the basis-set (Grieshop et al., 2009), the γ_e values determined here would be upper limits.

To model the evaporation of αP aerosol, the low-NO$_x$ volatility basis-set from Pathak et al. (2007a) and the ΔH_{vap} relationship from Epstein et al. (2009) were used; $\alpha_i = \{0.001, 0.012, 0.037, 0.088, 0.099, 0.25, 0.8\}$ and $C^* = \{0.01, 0.1, 1, 10, 100, 1000, 10^4\}\,\mu g\,m^{-3}$. We assume a fixed MW of 150 amu. Unlike the LO aerosol, the model results for αP aerosol do not agree with the observations in terms of the total aerosol MFR when $\gamma_e > 10^{-3}$. If γ_e is allowed to drop below 10^{-3} then approximate model/measurement agreement can be obtained. For reference, the mass thermograms for the individual model components are shown in Fig. 5c for the $\gamma_e = 10^{-4}$ case and predict clear distillation of molecular components in the αP aerosol

The determination of γ_e values from evaporation experiments, such as these, explicitly requires (i) a priori knowledge of a reasonably correct volatility basis-set and (ii) the assumption that the particles remain well-mixed throughout the evaporation process and therefore will exhibit volatility-dependent distillation. The lack of variability in the VUV mass spectra of αP aerosol with T_{TD} suggests that the second assumption may not be correct and thus that strict interpretation of the model-measurement agreement (or lack thereof) solely in terms of variations in γ_e may not be physically justifiable. Nonetheless, it is evident that when the LO and αP aerosol systems are modeled with the above assumptions, they have effective γ_e values that differ substantially from each other.

3.3 SOA as a glass?

Within the framework of traditional absorptive partitioning theory (Pankow, 1994; Odum et al., 1996; Donahue et al., 2006), OA volatility should be describable from the physical properties and relative abundances of the individual compounds comprising the aerosol. The results reported here for LO aerosol are consistent with this expectation. However, the αP observations are clearly not given that the VUV mass spectrum is essentially independent of T_{TD}. That the αP mass spectrum does not change with T_{TD} indicates that

the particle composition is homogenous, which suggests that the particle is well-mixed, at least initially. Yet, the observations also indicate the aerosol components do not evaporate according to their individual vapor pressures, which suggests minimal mixing, slow particle-phase diffusion and evaporation occurring in a "layer-by-layer" manner (assuming spherical particles).

To understand this result, we explore an alternative possibility, namely that the αP aerosol does not behave as a "subcooled" liquid (Marcolli et al., 2004; Cappa et al., 2008) during evaporation, but instead as a glass, wax or amorphous solid (Zobrist et al., 2008; Virtanen et al., 2010; Vaden et al., 2011) in which diffusion would be very slow. A few recent studies have indicated the potential for and importance of glassy organic aerosol in the atmosphere (Murray, 2008; Zobrist et al., 2008; Murray et al., 2010; Virtanen et al., 2010; Vaden et al., 2011). While most of these studies have been on aqueous organic glassy aerosol, as opposed to the non-aqueous system considered here, the Virtanen et al. results are for biogenic SOA at low ($\sim$30%) RH and the Vaden et al. (2010) results are for laboratory SOA and ambient OA. The key characteristic of a glass compared to a liquid is that diffusion in a glass is much slower. If particle-phase diffusion and mixing are sufficiently slow (compared to the timescale of the experiment) then the constituent compounds would not necessarily evaporate according to their Raoult's Law-adjusted vapor pressures, but rather evaporation would proceed in a layer-by-layer manner, without mixing to rehomogenize the particle and replenish the surface layer. In this case, the evaporation rate of the higher volatility components is limited by the rate at which surface sites become available, which in turn depends on the evaporation rate of the lower volatility components. This would appear as if the higher volatility compounds have an apparent γ_e much less than 1. Evaporation of the higher volatility compounds could leave the remaining lower volatility compounds at the surface to exist in a relatively high energy state (as neighbor molecules evaporate and are not replaced), thus causing the lower volatility material to evaporate somewhat faster than it might otherwise. The net result would be that the overall particle evaporation dynamics would likely appear somewhere between the highest and lowest volatility compounds, as has been observed for binary and ternary mixtures of solid dicarboxylic acids (C. D. Cappa, 2007). However, this description does not appear to apply to the αP aerosol here, because for γ_e values close to 1 even the least volatile components ($C^* = 10^{-2}\,\mu g\,m^{-3}$) are calculated to evaporate completely at temperatures lower than were observed.

For the residence time in the thermodenuder (15 s), if the particle-phase diffusivity were of the order $10^{-16}\,m^2\,s^{-1}$ then mixing would have been slow compared to the transit time through the thermodenuder. (Diffusion timescales were estimated as $t_d \sim r_p^2/D_p$, where D_p is the particle-phase diffusion coefficient and r_p is the particle radius.) Given that diffusion coefficients are temperature dependent, we conservatively estimate the OA diffusivity at ambient temperature would have needed to be $O(10^{-18}\,m^2\,s^{-1})$, corresponding to $t_d \sim 30$ min, to prevent mixing at all T_{TD}. For comparison, these values are similar to that observed for glassy organic polymers, such as $4 \times 10^{-18}\,m^2\,s^{-1}$ for iodohexane in polystyrene (Hui et al., 1987) or $3 \times 10^{-20}\,m^2\,s^{-1}$ for a small oligomer (640 g mol^{-1}) in polymethylmethacrylate (Bucknall et al., 2001). However, the highest T_{TD} are greater than typical glass transition temperatures, T_g, for some known low-MW glass formers, such as citric acid ($T_g = 289$ K), glucose ($T_g = 303$ K) or levoglucosan ($T_g \sim 284$ K) (Craig et al., 1999; Zobrist et al., 2008). This might indicate that particle-phase diffusion remains slow up to these high temperatures, but that the particles could not properly be considered as glassy. However, if high-MW oligomers form a significant fraction of the particle mass, higher T_g values are possible (although such a result seems inconsistent with our observed mass spectra). Nonetheless, the important physical parameter here is the particle-phase diffusivity (or viscosity); whether the OA particles are actually "glassy" is less important.

The LO aerosol is composed of numerous long chain hydrocarbons, which have only a few oxygenated functional groups (if any) per molecule. On the other hand, the αP aerosol is likely comprised of molecules having many functional groups (e.g. alcohols, ketones, aldehydes, carboxylic acids, etc.) per molecule and oligomeric species may also be formed (e.g. Gao et al., 2010). As such, the interactions between molecules in the LO aerosol will be dominated by van der Waals forces while in the αP aerosol the intermolecular interactions will be significantly more complex, likely with an important role for hydrogen bonding or further condensed phase reactions. We hypothesize that in the αP particles made here, these interactions are sufficiently strong that the net effect is to effectively retard mixing within the particle, thus giving rise to the observed behavior. However, this hypothesis must be reconciled with the observation that the particles were apparently compositionally homogenous, because if they were heterogeneous (e.g. with a composition that gradually changes from the core to the outermost shell) and glassy then the removal of outer layers would likely lead to an observable change in the particle composition (cf. Fig. 6e). Together, these findings suggest that a transformation occurred as the particles transited from the reaction flowtube to the thermodenuder, wherein the particles evolved from a more liquid-like state to a more arrested (potentially glassy) state leading to a dramatic, although perhaps continuous slow-down in particle-phase diffusion to the extent where the mixing timescale, t_d, is less than the TD residence time, and thus slow enough to prevent equilibration. Based on the experimental configuration, this conversion time scale is estimated as a few minutes. This may be related to the timescale associated with the formation of dimers, trimers, etc. through condensed phase or heterogeneous reactions, although there is no direct support for this from our experiments.

3.4 Sequential partitioning model

The formation and evolution of organic aerosol has, for the past two decades, been primarily understood through absorptive partitioning theory, generally with the assumption that partitioning occurs to the entire organic phase (or at least the entire secondary component). However, our observations for the αP aerosol suggest that traditional absorptive partitioning may not provide a robust description of the aerosol behavior because the particle-phase diffusion may change over time. In a first attempt to reconcile this traditional theory with our observations we postulate what we will term here a sequential equilibrium partitioning model (S-EPM). We emphasize that this is a conceptual model meant to demonstrate that traditional absorptive partitioning theory is not the only theory capable of describing aerosol growth experiments and that the S-EPM is not a definitive physical representation of the processes occurring in the experiments described here. The primary feature of the S-EPM that distinguishes it from traditional partitioning theory is that it is assumed that the aerosol is rapidly converted from an absorbing to a non-absorbing phase that does not participate in subsequent equilibrium partitioning. Aerosol growth in the S-EPM is modeled in a step-wise manner wherein the amount of material available for partitioning at every step in the simulation depends only on the available gas-phase material at that step since it is assumed that the OA formed in any previous step has been converted into non-absorptive material (i.e. glass) and is thus unavailable for partitioning. This can be thought of as allowing for the sequential formation of absorptive OA "shells" on top of a non-absorptive OA "core," and where the shells are continuously being converted into non-absorbing (e.g. glassy) OA. (The concept of "core" and "shell" allows for easy visualization of the process; however, we are not implying that the actual growth process must occur in this particular manner.) The S-EPM is therefore relevant to the above argument that absorbing (i.e. low viscosity) material is being converted to non-absorbing, glassy (i.e. high viscosity) material on some timescale. It is possible that the conversion to this non-absorbing phase involves the formation of oligomers. Because the S-EPM assumes that this process is occurring nearly instantaneously, the conversion process will directly influence the gas-particle partitioning behavior relative to traditional equilibrium models.

Consider a typical laboratory experiment in which a gas-phase organic compound is reacted with some oxidant (e.g. O_3, OH, NO_3). In the initial stages of the experiment, some small amount of hydrocarbon reacts (ΔHC) to produce a certain quantity of lower volatility products. The relative amount of any given reaction product depends upon the gas-phase yield of that compound. This newly produced gas-phase material can then partition to a new particle phase, leaving behind some amount of the gas-phase material that depends on the vapor pressure for that compound. In the S-EPM, it is assumed that the material that condensed to the particle phase in this step is "lost" from the system and does not influence partitioning in the next step, i.e. is converted to non-absorbing (non-partitioning) material (cf. Fig. 6a). In the next step, further hydrocarbon is reacted, producing more gas-phase material. The total material available for partitioning in this step is then the sum of the newly formed gas-phase material from reaction and the material from the previous step that did not condense (i.e. the residual gas-phase material). For compounds that partition strongly to the particle phase, the new total is effectively equal to only the material produced from gas-phase reactions, while for compounds that weakly partition to the particle phase the total is equal to the sum of the newly produced and residual gas-phase material. Overall, this can be expressed as:

$$C_{g,n,i}^{rxn} = \alpha_i \cdot \Delta HC_n, \tag{2}$$

$$C_{g,i,n}^{res} = C_{tot,i,n} - C_{p,i,n}, \tag{3}$$

$$C_{tot,i,n+1} = C_{g,i,n+1}^{rxn} + C_{g,i,n}^{res}, \tag{4}$$

where $C_{g,i}^{rxn}$ is the gas-phase concentration produced from reaction of the parent hydrocarbon, α_i is the gas-phase yield, $C_{g,i}^{res}$ is the residual gas-phase concentration, $C_{tot,i}$ is the total concentration of material available for partitioning, $C_{p,i}$ is the particle-phase concentration, i indicates different components and n indicates the step. Note that the total material available for partitioning at a given step, $C_{tot,i,n}$, is just the gas-phase material because we have assumed that the particle phase material from previous steps has become non-absorbing and is therefore no longer counted in the total. At each step the newly formed particle phase material is then:

$$C_{p,i,n} = \xi_i C_{tot,i,n} \tag{5}$$

$$\xi_{i,n} = \left(1 + \frac{C_i^*}{C_{OA,n}}\right)^{-1} ; C_{OA,n} = \sum_i \xi_{i,n} C_{tot,i,n} \tag{6}$$

where C_i^* is the saturation concentration of compound i and $C_{OA,n}$ only includes the absorptive material. The total OA produced throughout the experiment is then:

$$C_{OA,tot} = \sum_n C_{OA,n}. \tag{7}$$

The sequential absorption model has been tested to determine to what extent it is consistent with laboratory aerosol growth experiments, which universally show that the aerosol yield increases non-linearly with increasing $C_{OA,tot}$ (where the aerosol yield is defined as $C_{OA,tot}/\Delta HC_{tot}$ and ΔHC_{tot} is the total reacted hydrocarbon, i.e. the sum of the ΔHC_n values). Here, the S-EPM has been developed following from the aerosol basis-set framework, wherein the compounds are represented in logarithmically spaced bins with respect to their saturation concentrations (Donahue et al., 2006). The only adjustable parameters are the α_i yield values for each component in the basis-set since the products are assumed to be
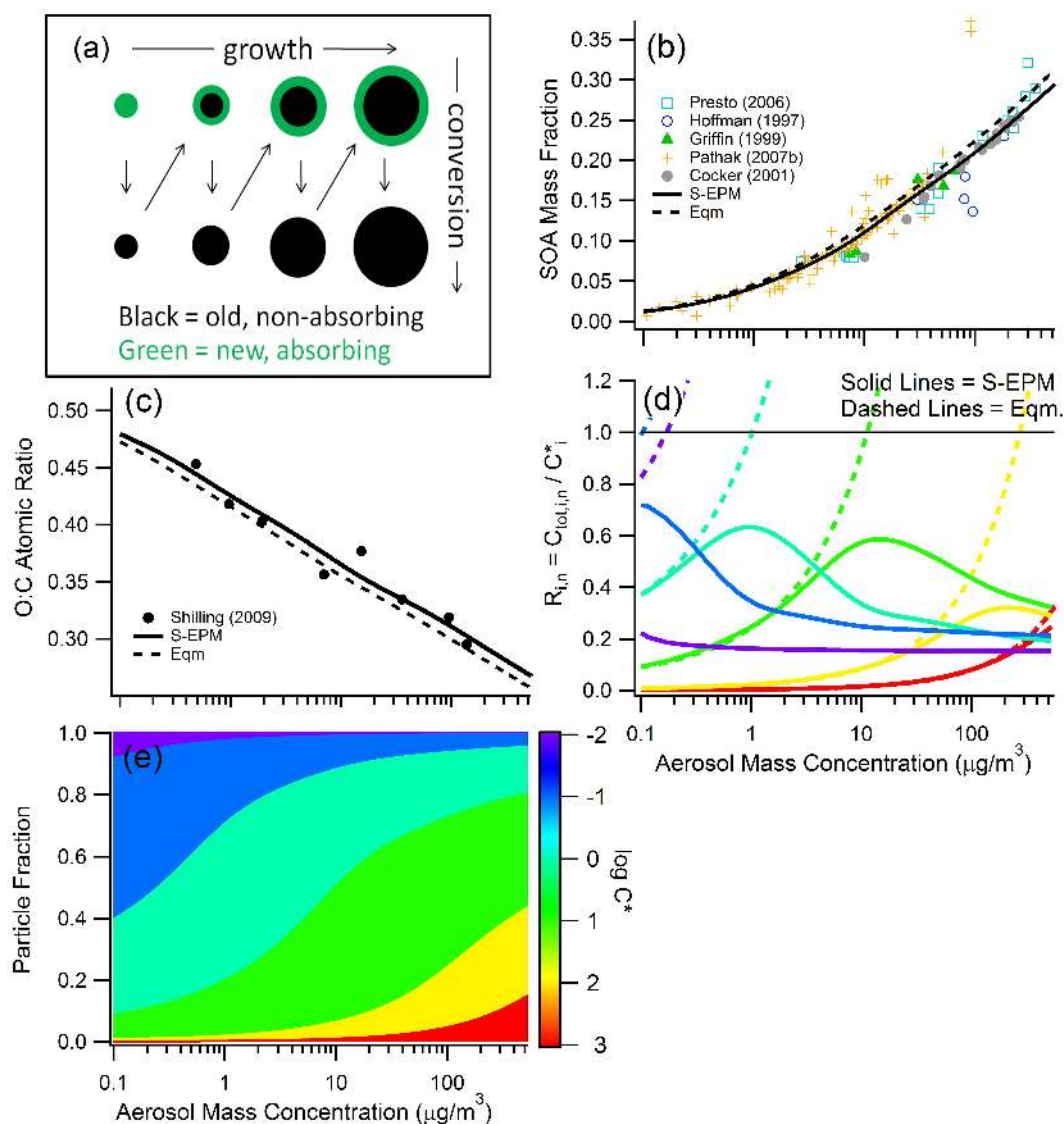
Fig. 6. (a) A schematic of the processes in the S-EPM. Up to down (and green to black) represents conversion of the previously absorbing phase into a non-absorbing (glassy) phase. Diagonal (down-to-up/left-to-right) represents particle growth and the formation of a new absorbing phase. **(b)** The calculated aerosol yield from the sequential partitioning model is shown (solid line) along with the measurements for α-Pinene + O_3 from Hoffman et al. (1997); Griffin et al. (1999); Cocker et al. (2001); Presto et al. (2006), and Pathak et al. (2007b). Results from a traditional equilibrium partitioning model using the same volatility basis-set as for the S-EPM are shown for comparison (dashed line). **(c)** The calculated O:C from the S-EPM (solid line) and the equilibrium (dashed line) models are shown along with the observations from Shilling et al. (2009). Note that the variation in O:C with C^* has been adjusted to give good model/measurement agreement. **(d)** The calculated variation in $R_{i,n}$, i.e. the total mass concentration of each compound relative to its saturation concentration, as a function of C_{OA} for both the S-EPM (solid lines) and the traditional model (dashed lines). Only material available for partitioning is included in $C_{tot,i,n}$. Line colors indicate components with different C^*, and are given in the color bar. **(e)** The relative particle fraction of each compound as a function of C_{OA}. Colors correspond to C^*.

non-reactive. As a specific test-case, we use the aerosol yield measurements for αP aerosol determined from a number of different studies as presented by Pathak et al. (2007a): Hoffmann et al. (1998), Griffin et al. (1999), Cocker et al. (2001), Presto et al. (2006), and Pathak et al. (2007b). A 6-product volatility basis-set, ranging from $C^* = 10^{-2}$ to $10^3 \, \mu g \, m^{-3}$,

has been used and α_i values determined by minimizing the residual between the calculated and measured aerosol yield. The S-EPM is capable of explaining the aerosol yield observations (Fig. 6b), with a best-fit α_i basis-set = {0.001, 0.012, 0.045, 0.11, 0.10, 0.18}. Note that the calculated aerosol yield curves are nearly insensitive to the ΔHC_n step size

used, although the calculated amount of added aerosol mass at each step ($C_{OA,n}$) is sensitive to the ΔHC_n used, with smaller $C_{OA,n}$ corresponding to smaller ΔHC_n values.

The evolution of the fractional contributions of the individual components to the total aerosol mass as a function of $C_{OA,tot}$ provides some insights into how the particle composition will change. As expected, at low $C_{OA,tot}$ the composition is dominated by the lower volatility material and, as $C_{OA,tot}$ increases, the contributions of the higher volatility material increase (Fig. 6e). Comparison with the calculated total (gas + particle) concentration of each compound relative to the saturation concentration of that compound ($R_{i,n} = C_{tot,i,n}/C_i^*$) indicates that this ratio is a primary factor driving the evolution of the particle composition (Fig. 6d). Recalling that the definition of $C_{tot,i,n}$ excludes the OA that has been converted to non-absorbing material, the variation of $R_{i,n}$ for the S-EPM is seen to be quite different than for the traditional model, in which $R_{i,n}$ continuously increases as more material is produced from gas-phase oxidation of the parent compound (Fig. 6d). The specific shape of the $R_{i,n}$ vs. C_{OA} trajectories for the S-EPM results from a balance between production of new gas-phase material and the loss of condensed-phase material via conversion to the non-absorbing phase. The fraction that will partition to the condensed-phase at any step is governed both by the individual C_i^* values and the available $C_{tot,i}$ (the combination of which determines the amount of newly formed OA; cf. Eqs. 1 and 6). As $C_{tot,i,n}$ increases for a given component, more of that component will go to the condensed phase in a given step, and thus a greater fraction will be "lost" via conversion to a non-absorbing phase. When the fraction of an individual component that partitions to the condensed-phase in a given step is less than 50%, $C_{tot,i}$ will build up with each step. However, once that fraction exceeds 50%, material is lost to the conversion process faster than it is formed from gas-phase reactions, and accordingly $R_{i,n}$ begins to decrease.

This variation in the overall particle composition with $C_{OA,tot}$ can be used to examine how, for example, the particle O:C ratio might change as a function of $C_{OA,tot}$ during growth experiments, as was measured by Shilling et al. (2009). Here, we assume that any condensed-phase reactions that occur preserve the overall O:C, which is equivalent to saying that there is no mass-loss from the particle due to any such reactions. However, even if the compounds were to lose their chemical identity during the conversion process, an assumption of no mass loss means that the overall O:C can be determined by keeping track of the variation in the individual components;

$$(O:C)_{total,n} = \sum_i (O:C)_i \frac{C_{p,i,n}}{C_{OA,n}}. \quad (8)$$

If it is assumed that O:C for the binned components varies linearly with log C^*, with higher O:C corresponding to lower C^* components, then it is possible to match the observations from Shilling et al. (2009) (Fig. 6c). The specific relationship determined here was O:C $= -0.025 + 0.11(4 - \log C^*)$, which yields values reasonably similar to those derived by Shilling et al. (2009) using a 4-product equilibrium partitioning model. Thus, the S-EPM is capable of explaining OA growth experiments in terms of both the observed mass yields and O:C values.

The results from the S-EPM can be compared to a traditional equilibrium absorption model, in which the entire OA mass influences the partitioning at every step. For the same α_i basis-set as determined for the S-EPM the aerosol yield curve for the traditional model gives very similar results, with only a slightly higher aerosol yield for a given $C_{OA,tot}$ (Fig. 6b). Thus, in the context of aerosol growth experiments these two models do not differ significantly in terms of the derived α_i basis-sets. The difference is primarily that, in the S-EPM, incorporation of the higher volatility components is delayed until their abundance is larger (i.e. more of the parent hydrocarbon has reacted) because there is only a small amount of condensed-phase material available into which it can partition at any given step and the actual concentration is too far below the saturation concentration (Fig. 6d). This suggests that the production rate of the individual components from gas-phase reactions is an important controlling factor. However, even though the S-EPM and the traditional model yield essentially the same results (e.g. volatility basis-sets), the key feature is that there will be a real difference in the physical outcome for the OA, as the S-EPM model allows for formation of OA in which much of the OA mass is non-absorbing and, perhaps, glassy. Subsequent evaporation of the OA formed from the traditional model and the S-EPM, induced either by dilution or heating, may therefore proceed along different paths than would be predicted using the α_i/volatility basis-sets determined from the growth experiments. In other words, although it is possible to describe OA growth through equilibrium partitioning theory the thus derived properties may not ultimately provide an accurate description of the effective thermodynamic properties of the formed OA.

One potential and important difficulty associated with applying the S-EPM to the interpretation of the αP results in this study is that the S-EPM, unlike the equilibrium model, could lead to a situation where the thus formed particles are composed of sequential layers that have differing composition, with a greater fractional amount of higher volatility material in the outer layers than in the inner layers. This is a result of the "shell-by-shell" formation in the S-EPM, whereas in the equilibrium model it is assumed that the particles are well-mixed at all times. (Although we note that there is nothing inherent to the S-EPM that requires shell-by-shell formation, only that the absorbing material is converted to a non-absorbing phase.) However, the observations suggest that the αP particles are homogeneous, yet highly viscous such that the particle composition does not change during evaporation. As such, we reiterate that the S-EPM is not meant to provide

an exact representation of the physical processes that actually occur in our experiments, but only to demonstrate that aerosol growth measurements can be modeled within a conceptual framework that allows for transformation of the particles from a liquid-like to glassy phase on some timescale.

An alternative possibility is that the particles are not "glassy", but are actually composed of a high fraction of essentially non-volatile oligomeric compounds and that, during evaporation, we are actually seeing the release of monomers of constant average composition (e.g. monomer-by-monomer evaporation). Although our VUV mass spectra suggests that oligomers are only a small fraction of the total SOA mass, we cannot rule out the possibility that oligomers fall apart in the VUV-MS, thus appearing primarily as their monomers (or fragments thereof). If this is the case, it may be that the formation of (non-volatile) oligomers on a relatively rapid timescale is what drives the discrepancy between growth and evaporation experiments. However, such a process requires no fundamental change to the SPM as described above, so long as one posits that the oligomeric mass is a "non-absorbing" phase.

3.5 Comparison with literature observations

3.5.1 Laboratory experiments

Our observations of αP aerosol evaporation indicate that the individual compounds comprising the aerosol are not distilled from the particles according to their volatility as they are heated. However, not all laboratory-generated OA appears to behave in this manner. For example, the work by Ziemann and co-workers indicates that many gas-phase reactions lead to secondary OA in which distillation occurs while other reactions are more consistent with the observations presented here (Docherty et al., 2005; Gong et al., 2005; Lim and Ziemann, 2005, 2009). For example, their experiments using αP aerosol (formed with cyclohexane, an OH radical scavenger, present) show the OA to have very low volatility components, similar to the observations presented here, but, in contrast, they also observed evidence for distillation in their mass thermograms (Docherty et al., 2005). Further, in-chamber dilution experiments by Grieshop et al. (2007) provide evidence for changes to the particle composition upon evaporation. It may be that the longer timescales available during the evaporation process in these previous experiments compared to our experiments are an important consideration.

Kostenidou et al. (2009) measured mass spectra of αP aerosol behind a TD using an EI-AMS. Depending on the explicit conditions (high vs. low NO_x, low vs. high RH), they found some variation in the observed mass spectrum with T_{TD}, which suggests chemical changes upon heating, inconsistent with our observations. However, the αP aerosol in their experiments was overall significantly more volatile than in our experiments, as evidenced by the VFR falling to 0.1 by 60–70 °C in their experiments compared to around 120 °C in

ours (for approximately the same TD residence time, but with an initial $C_{OA} \sim 5 - 10$ times smaller in their experiments), which indicates that the αP particles in these experiments may not be directly comparable. Our VFR vs. T_{TD} observations for αP aerosol are, however, consistent with results from smog-chamber experiments by Huffman et al. (2009b) (with the same residence time and similar C_{OA} as here). Besides the different C_{OA}, a difference between the Kostenidou et al. (2009) results and ours and the Huffman et al. results is that Kostenidou et al. (2009) used an OH scavenger. In addition to modifying the chemistry that occurs in the gas-phase, the presence of OH radicals could lead to heterogeneous reactions that could modify the particle composition directly (e.g. Smith et al., 2009). However, large differences between mass thermograms measured for αP + O_3 aerosol formed with/without an OH scavenger present have not been observed (Jonsson et al., 2007), which suggests that the presence/absence of an OH scavenger may not be the main reason for the observed differences in the VFR curves. Finally, another difference is that in the Kostenidou et al. (2009) experiments the αP aerosol was formed over many hours in a smog chamber whereas our αP aerosol was formed in a few minutes in a flow tube (although we note that the Huffman et al. (2009b) αP aerosol was also formed over many hours). Certainly, there remains an unexplained inconsistency given that these different experiments all probed αP aerosol evaporation over similar timescales in a TD.

Shilling et al. (2009) investigated how the O:C atomic ratio of αP particles varied with mass loading for aerosol growth experiments, finding that O:C at very low mass loadings was larger than at high loadings. Although their experiments showed that the composition of αP particles does vary with mass loading, Shilling et al. (2009) determined how composition varied with increasing mass loading (i.e. as the particles grew) and not how composition changed once already formed particles evaporated; thus, our experiments may not be directly comparable. Nonetheless, our VUV-AMS measurements provide compelling evidence that under some cases OA volatility does not follow from traditional partitioning theory. Our overall conclusion, that the αP SOA exists as an amorphous solid while the LO aerosol is liquid-like, is consistent with the observations of Virtanen et al. (2010) who concluded based on measurements of particle bounce that biogenic SOA (similar to the αP SOA here) was glassy and of Vaden et al. (2011), who observed slow evaporation kinetics for chamber and field OA particles.

3.5.2 Field observations

Comparison of our laboratory results with field observations is somewhat challenging because of the complications introduced by the ambient OA potentially existing as an external mixture of different OA aerosol types. With an external mixture, it is possible that T-dependent changes to the observed total OA spectrum could be driven by differences

in volatility between externally mixed OA types and not by chemical changes within a specific (internally mixed) aerosol type. With this caveat in mind, we find that our laboratory observations for αP aerosol are generally consistent with recent ambient observations of T-dependent OA mass spectra during the FAME-2008 campaign (Hildebrandt et al., 2010), wherein statistically insignificant differences in the average OA mass spectrum were observed between ambient temperature and $T_{TD} = 110\,^\circ$C or $145\,^\circ$C. The total OA mass during FAME-2008 was dominated by highly oxygenated organic aerosol (OOA; O:C $\sim$ 0.77) with no measurable contribution from "hydrocarbon-like" OA (HOA). In contrast, during the SOAR and MILAGRO campaigns, variations in the campaign average O:C ratio for OA with T_{TD} were observed (Huffman et al., 2009a), which could be interpreted as indicating distillation of compounds with lower O:C (and presumably higher volatility) from the OA particles occurred. However, we find that the variation in O:C with T_{TD} during these two campaigns can be reasonably well explained if one assumes that the various identified OA types (e.g. HOA, OOA, etc.) have a T-independent (but unique) O:C but where the fractional contribution of each component varies with temperature (Appendix A). As such, the variation in O:C with T_{TD} during MILAGRO and SOAR may be driven by changes in the relative amount of each aerosol type and not necessarily by changes in the chemical makeup of each aerosol type.

The volatility of the ambient OA observed during MILAGRO as deduced from tandem TD-AMS experiments has recently been quantified under the assumption that the OA was describable through absorptive partitioning theory (i.e. remained well-mixed throughout evaporation) (Cappa and Jimenez, 2010). It was demonstrated that a significant fraction of the OA could be considered "non-volatile," and that the ambient OA was significantly less volatile than typical laboratory-generated SOA. However, if the ambient OA did not actually remain well-mixed, but instead acted as a glassy substance with slow diffusion, akin to the αP particles considered here and in Virtanen et al. (2010), then the interpretation in terms of partitioning theory is not physically justifiable even though the data may be well represented. This does not necessarily mean that ambient OA volatility cannot be parameterized as a 1, 2...n component system within the framework of partitioning theory, only that the derived properties may not have a readily interpretable physical or chemical meaning.

3.5.3 The evaporation coefficient

Above, we used a kinetic model of aerosol evaporation in a TD (Cappa, 2010) to deduce that the evaporation coefficient for LO aerosol is on the order of 0.5 ($0.1 < \gamma_e < 1$). However, it has previously been suggested based on room-temperature isothermal dilution experiments that the evaporation coefficient, γ_e, for LO aerosol is 0.001–0.01 (Grieshop

et al., 2009). Our results are inconsistent with such a low value for γ_e for LO aerosol. As discussed in Sect. 3.2, a different volatility/ΔH_{vap} distribution pair has been used here than in Grieshop et al. (2009). However, we find that if the original volatility/ΔH_{vap} distribution pair is used this general conclusion does not change. Additionally, we observed that the LO particles evaporated significantly in the activated carbon denuder section of the TD. Using the volatility distribution given by Grieshop et al. (2009) for diesel aerosol, we calculate that if $\gamma_e < 0.01$ then the VFR for LO aerosol at ambient temperature should have remained above 0.98, which is also inconsistent with our observations. These low-temperature results are important, as they demonstrate that the differences between the LO and αP particles are not being driven by condensed-phase chemistry occurring at elevated temperatures.

In a separate study using the same isothermal dilution methodology, Grieshop et al. (2007) also determined that $0.001 < \gamma_e < 0.01$ for αP aerosol. In this case, we similarly find that the effective γ_e for αP aerosol is significantly less than 1, with $\gamma_e = 10^{-4}$ based on the TD measurements. The reason for the very different level of agreement between the LO and αP aerosol in our TD experiments compared to the isothermal dilution experiments (Grieshop et al., 2007, 2009) is not clear, although could be related to the timescales associated with evaporation vs. loss of gas-phase species to the chamber walls (Loza et al., 2010; Matsunaga and Ziemann, 2010). We note that if our results for the LO aerosol are correct, this calls into question the robustness of the methodology used by Grieshop et al. to estimate γ_e values in general (Grieshop et al., 2007, 2009).

4 Implications

The formation and evolution of OA in the atmosphere has traditionally been described through equilibrium partitioning theory. However, our results suggest that the thermodynamic properties of OA as deduced from aerosol yield experiments may not be directly applicable to the thus formed OA. In particular, it appears that the volatility of SOA may be significantly lower than would be expected from the aerosol yield experiments. This suggests that SOA in the atmosphere may then exhibit a significantly lower sensitivity, or at least a significantly slower response, to dilution and changes in temperature than expected. In the limit of considering the SOA to be completely non-volatile at typical ambient temperatures, this would therefore allow for a much greater amount of SOA to be preserved downwind of strong sources because the SOA would not evaporate upon dilution. However, at the same time our results suggest that POA (here, in the form of LO aerosol) would be quite sensitive to dilution and thus POA mass concentrations would decrease from evaporation upon dilution (in addition to the influence of dilution itself).

Volkamer et al. (2006) found that the magnitude of the discrepancy between model and measured SOA increases with photochemical age. To the extent that photochemical age is correlated with dilution, having a non-volatile (or very low volatility) SOA would push model estimates up, thus helping to reduce the model/measurement discrepancy. Consider, for example, the 2-product volatility of αP aerosol as determined by Griffin et al. (1999), where $C_1^* = 5.84\,\mu g\,m^{-3}$ and $C_2^* = 250\,\mu g\,m^{-3}$ and $\alpha_1 = 0.038$ and $\alpha_2 = 0.326$. If one assumes that enough α-pinene reacts to produce $10\,\mu g\,m^{-3}$ of OA, dilution by a factor of 2 would cause the OA concentration to decrease to $0.5\,\mu g\,m^{-3}$, where evaporation has caused a further loss of 90% of the OA mass ($4.5\,\mu g\,m^{-3}$ out of the $5\,\mu g\,m^{-3}$ remaining after dilution). However, if the volatility of the αP were much lower, then the actual loss of OA mass from dilution would decrease by a significant amount. Finally, the slower diffusion in a glassy particle compared to a liquid-like particle could strongly affect the processes and timescales associated with heterogeneous chemical reactions on SOA particles (Zahardis and Petrucci, 2007).

Appendix A

Ambient O:C atomic ratios

The O:C values as a function of T_{TD} during SOAR and MILAGRO have been estimated using the data presented in (Huffman et al., 2009a). For simplicity, the analysis has been limited to considering the total OA to only be comprised of three distinct OA types, or factors: a hydrocarbon-like OA (HOA), a low-volatility oxygenated OA (LV-OOA) and a high-volatility oxygenated OA (HV-OOA). Other component factors (e.g. biomass burning OA or "local" OA) were assumed to have the same properties as HOA. The relative amounts of the HOA, LV-OOA and HV-OOA components at each T_{TD} were determined from Fig. S8 in Huffman et al. (2009a). The average O:C was then calculated by multiplying each of the relative OA contributions by the O:C for that factor and summing:

$$O:C_{tot}(T_{TD}) = \sum_i f_i(T_{TD}) \times O:C_i \qquad (A1)$$

where f_i is the fractional amount of each factor at each T_{TD} and O:C$_i$ is the O:C for each factor. We assume that O:C$_i$ for each factor is temperature independent. The difference between the observed O:C and the calculated O:C was minimized at all temperatures to determine an effective O:C$_i$ for the LV-OOA and HV-OOA components, and HOA was assumed to be 0.1 (Ng et al., 2010). This results in derived O:C values for the LV-OOA component of 0.56 (MILAGRO) and 0.69 (SOAR) and for the HV-OOA component of 0.45 (MILAGRO) and 0.21 (SOAR). The values deduced here for SOAR are similar to those reported by Ng et al. (Ng et al.,

2010); 0.84 (LV-OOA) and 0.26 (HV-OOA). No comparable values are available for MILAGRO, although the average OOA O:C was ~0.53 (Ng et al., 2010), consistent with our finding.

Edited by: Neil M. Donahue

References

An, W. J., Pathak, R. K., Lee, B. H., and Pandis, S. N.: Aerosol volatility measurement using an improved thermodenuder: Application to secondary organic aerosol, J. Aerosol. Sci., 38, 305–314, 2007.

Bucknall, D. G., Higgins, J. S., and Butler, S. A.: Early stages of oligomer-polymer diffusion, Chem. Eng. Sci., 56, 5473–5483, doi:10.1016/s0009-2509(01)00171-3, 2001.

Cappa, C. D.: A model of aerosol evaporation kinetics in a thermodenuder, Atmos. Meas. Tech., 3, 579–592, doi:10.5194/amt-3-579-2010, 2010.

Cappa, C. D. and Jimenez, J. L.: Quantitative estimates of the volatility of ambient organic aerosol, Atmos. Chem. Phys., 10, 5409–5424, doi:10.5194/acp-10-5409-2010, 2010.

Cappa, C. D., Lovejoy, E. R., Ravishankara, A. R.: Evaporation behavior of mixtures of organic and inorganic compounds, unpublished data, 2007.

Cappa, C. D., Lovejoy, E. R., and Ravishankara, A. R.: Evidence for liquid-like and nonideal behavior of a mixture of organic aerosol components, P. Natl. Acad. Sci. USA, 105, 18687–18691, doi:10.1073/pnas.0802144105, 2008.

Cocker, D. R., Clegg, S. L., Flagan, R. C., and Seinfeld, J. H.: The effect of water on gas-particle partitioning of secondary organic aerosol. Part I: alpha-pinene/ozone system, Atmos. Environ., 35, 6049–6072, 2001.

Craig, D. Q. M., Royall, P. G., Kett, V. L., and Hopton, M. L.: The relevance of the amorphous state to pharmaceutical dosage forms: glassy drugs and freeze dried systems, Int. J. Pharm., 179, 179–207, doi:10.1016/s0378-5173(98)00338-x, 1999.

Docherty, K. S., Wu, W., Lim, Y. B., and Ziemann, P. J.: Contributions of organic peroxides to secondary aerosol formed from reactions of monoterpenes with O_3, Environ. Sci. Technol., 39, 4049–4059, doi:10.1021/es050228s, 2005.

Donahue, N. M., Robinson, A. L., Stanier, C. O., and Pandis, S. N.: Coupled partitioning, dilution, and chemical aging of semivolatile organics, Environ. Sci. Technol., 40, 2635–2643, doi:10.1021/es052297c, 2006.

Dzepina, K., Volkamer, R. M., Madronich, S., Tulet, P., Ulbrich, I. M., Zhang, Q., Cappa, C. D., Ziemann, P. J., and Jimenez, J. L.: Evaluation of recently-proposed secondary organic aerosol models for a case study in Mexico City, Atmos. Chem. Phys., 9, 5681–5709, doi:10.5194/acp-9-5681-2009, 2009.

Epstein, S. A., Riipinen, I., and Donahue, N. M.: A Semiempirical Correlation between Enthalpy of Vaporization and Saturation Concentration for Organic Aerosol, Environ. Sci. Technol., 44, 743–748, doi:10.1021/es902497z, 2009.

Gao, Y., Hall, W. A., and Johnston, M. V.: Molecular Composition of Monoterpene Secondary Organic Aerosol at Low Mass Loading, Environ. Sci. Technol., 44, 7897–7902, doi:10.1021/es101861k, 2010.

Gong, H. M., Matsunaga, A., and Ziemann, P. J.: Products and mechanism of secondary organic aerosol formation from reactions of linear alkenes with NO$_3$ radicals, J. Phys. Chem. A, 109, 4312–4324, 2005.

Grieshop, A. P., Donahue, N. M., and Robinson, A. L.: Is the gas-particle partitioning in alpha-pinene secondary organic aerosol reversible?, Geophys. Res. Lett., 34, L14810, doi:10.1029/2007GL029987, 2007.

Grieshop, A. P., Miracolo, M. A., Donahue, N. M., and Robinson, A. L.: Constraining the Volatility Distribution and Gas-Particle Partitioning of Combustion Aerosols Using Isothermal Dilution and Thermodenuder Measurements, Environ. Sci. Technol., 43, 4750–4756, doi:10.1021/es8032378, 2009.

Griffin, R. J., Cocker, D. R., Flagan, R. C., and Seinfeld, J. H.: Organic aerosol formation from the oxidation of biogenic hydrocarbons, J. Geophys. Res.-Atmos, 104, 3555–3567, doi:10.1029/1998JD100049, 1999.

Heald, C. L., Jacob, D. J., Park, R. J., Russell, L. M., Huebert, B. J., Seinfeld, J. H., Liao, H., and Weber, R. J.: A large organic aerosol source in the free troposphere missing from current models, Geophys. Res. Lett., 32, L18809, doi:18810.11029/12005GL023831, 2005.

Hildebrandt, L., Engelhart, G. J., Mohr, C., Kostenidou, E., Lanz, V. A., Bougiatioti, A., DeCarlo, P. F., Prevot, A. S. H., Baltensperger, U., Mihalopoulos, N., Donahue, N. M., and Pandis, S. N.: Aged organic aerosol in the Eastern Mediterranean: the Finokalia Aerosol Measurement Experiment - 2008, Atmos. Chem. Phys., 10, 4167–4186, doi:10.5194/acp-10-4167-2010, 2010.

Hoffmann, T., Odum, J. R., Bowman, F., Collins, D., Klockow, D., Flagan, R. C., and Seinfeld, J. H.: Formation of organic aerosols from the oxidation of biogenic hydrocarbons, J. Atmos. Chem., 26, 189–222, 1997.

Hoffmann, T., Bandur, R., Marggraf, U., and Linscheid, M.: Molecular composition of organic aerosols formed in the α-pinene/O$_3$ reaction: Implications for new particle formation processes, J. Geophys. Res.-Atmos., 103, 25569–25578, doi:10.1029/98JD01816, 1998.

Huffman, J. A., Ziemann, P. J., Jayne, J. T., Worsnop, D. R., and Jimenez, J. L.: Development and characterization of a fast-stepping/scanning thermodenuder for chemically-resolved aerosol volatility measurements, Aerosol Sci. Technol., 42, 395–407, 2008.

Huffman, J. A., Docherty, K. S., Aiken, A. C., Cubison, M. J., Ulbrich, I. M., DeCarlo, P. F., Sueper, D., Jayne, J. T., Worsnop, D., Ziemann, P. J., and Jimenez, J. L.: Chemically-Resolved volatility measurments from two megacity field studies, Atmos. Chem. Phys., 9, 7161–7182, doi:10.5194/acp-9-7161-2009, 2009a.

Huffman, J. A., Docherty, K. S., Mohr, C., Cubison, M. J., Ulbrich, I. M., Ziemann, P. J., Onasch, T. B., and Jimenez, J. L.: Chemically-Resolved Volatility Measurements of Organic Aerosol from Different Sources, Environ. Sci. Technol., 43,

5351–5357, 2009b.

Hui, C. Y., Wu, K. C., Lasky, R. C., and Kramer, E. J.: Case-II diffusion in polymers. II. Steady-state front motion, Journal of Applied Physics, 61, 5137–5149, doi:10.1063/1.338288, 1987.

IPCC: Climate Change, in: The Physical Science Basis – Contribution of Working Group I to the Fourth Assessment Report of the Intergovernmental Panel on Climate Change, edited by: Solomon, S., Qin, D., and Manning, M., Cambridge University Press, Cambridge, 996 pp., 2007.

Jonsson, A. M., Hallquist, M., and Saathoff, H.: Volatility of secondary organic aerosols from the ozone initiated oxidation of alpha-pinene and limonene, J. Aerosol. Sci., 38, 843–852, 2007.

Kostenidou, E., Lee, B. H., Engelhart, G. J., Pierce, J. R., and Pandis, S. N.: Mass Spectra Deconvolution of Low, Medium, and High Volatility Biogenic Secondary Organic Aerosol, Environ. Sci. Technol., 43, 4884–4889, doi:10.1021/es803676g, 2009.

Lambe, A. T., Miracolo, M. A., Hennigan, C. J., Robinson, A. L., and Donahue, N. M.: Effective Rate Constants and Uptake Coefficients for the Reactions of Organic Molecular Markers (n-Alkanes, Hopanes, and Steranes) in Motor Oil and Diesel Primary Organic Aerosols with Hydroxyl Radicals, Environ. Sci. Technol., 43, 8794–8800, doi:10.1021/es901745h, 2009.

Lane, T. E., Donahue, N. M., and Pandis, S. N.: Simulating secondary organic aerosol formation using the volatility basis-set approach in a chemical transport model, Atmos. Environ., 42, 7439–7451, doi:10.1016/j.atmosenv.2008.06.026, 2008.

Lide, D. R.: CRC Handbook of Chemistry and Physics, 86th ed., CRC Press, Boca Raton, FL, 2005.

Lim, Y. B. and Ziemann, P. J.: Products and mechanism of secondary organic aerosol formation from reactions of n-alkanes with OH radicals in the presence of NO$_x$, Environ. Sci. Technol., 39, 9229–9236, doi:10.1021/es051447g, 2005.

Lim, Y. B. and Ziemann, P. J.: Chemistry of Secondary Organic Aerosol Formation from OH Radical-Initiated Reactions of Linear, Branched, and Cyclic Alkanes in the Presence of NO$_x$, Aerosol Sci. Technol., 43, 604–619, 2009.

Loza, C. L., Chan, A. W. H., Galloway, M. M., Keutsch, F. N., Flagan, R. C., and Seinfeld, J. H.: Characterization of Vapor Wall Loss in Laboratory Chambers, Environ. Sci. Technol., 44, 5074–5078, doi:10.1021/es100727v, 2010.

Marcolli, C., Luo, B. P., and Peter, T.: Mixing of the organic aerosol fractions: Liquids as the thermodynamically stable phases, J. Phys. Chem. A, 108, 2216–2224, 2004.

Matsunaga, A. and Ziemann, P. J.: Gas-Wall Partitioning of Organic Compounds in a Teflon Film Chamber and Potential Effects on Reaction Product and Aerosol Yield Measurements, Aerosol Sci. Technol., 44, 881–892, doi:10.1080/02786826.2010.501044, 2010.

Murray, B. J.: Inhibition of ice crystallisation in highly viscous aqueous organic acid droplets, Atmos. Chem. Phys., 8, 5423–5433, doi:10.5194/acp-8-5423-2008, 2008.

Murray, B. J., Wilson, T. W., Dobbie, S., Cui, Z., Al-Jumur, S. M. R. K., Mohler, O., Schnaiter, M., Wagner, R., Benz, S., Niemand, M., Saathoff, H., Ebert, V., Wagner, S., and Karcher, B.: Heterogeneous nucleation of ice particles on glassy aerosols under cirrus conditions, Nat. Geosci., 3, 233–237, 2010.

Mysak, E. R., Wilson, K. R., Jimenez-Cruz, M., Ahmed, M., and Baer, T.: Synchrotron radiation based aerosol time-of-flight mass spectrometry for organic constituents, Anal. Chem., 77, 5953–

5960, 2005.

Ng, N. L., Kroll, J. H., Keywood, M. D., Bahreini, R., Varut-bangkul, V., Flagan, R. C., Seinfeld, J. H., Lee, A., and Goldstein, A. H.: Contribution of first- versus second-generation products to secondary organic aerosols formed in the oxidation of biogenic hydrocarbons, Environ. Sci. Technol., 40, 2283–2297, doi:10.1021/es052269u, 2006.

Ng, N. L., Canagaratna, M. R., Zhang, Q., Jimenez, J. L., Tian, J., Ulbrich, I. M., Kroll, J. H., Docherty, K. S., Chhabra, P. S., Bahreini, R., Murphy, S. M., Seinfeld, J. H., Hildebrandt, L., Donahue, N. M., DeCarlo, P. F., Lanz, V. A., Prévôt, A. S. H., Dinar, E., Rudich, Y., and Worsnop, D. R.: Organic aerosol components observed in Northern Hemispheric datasets from Aerosol Mass Spectrometry, Atmos. Chem. Phys., 10, 4625–4641, doi:10.5194/acp-10-4625-2010, 2010.

Odum, J. R., Hoffmann, T., Bowman, F., Collins, D., Flagan, R. C., and Seinfeld, J. H.: Gas/particle partitioning and secondary organic aerosol yields, Environ. Sci. Technol., 30, 2580–2585, 1996.

Pankow, J. F.: An Absorption-Model of the Gas Aerosol Partitioning Involved in the Formation of Secondary Organic Aerosol, Atmos. Environ., 28, 189–193, 1994.

Pathak, R. K., Presto, A. A., Lane, T. E., Stanier, C. O., Donahue, N. M., and Pandis, S. N.: Ozonolysis of α-pinene: parameterization of secondary organic aerosol mass fraction, Atmos. Chem. Phys., 7, 3811–3821, doi:10.5194/acp-7-3811-2007, 2007a.

Pathak, R. K., Stanier, C. O., Donahue, N. M., and Pandis, S. N.: Ozonolysis of alpha-pinene at atmospherically relevant concentrations: Temperature dependence of aerosol mass fractions (yields), J. Geophys. Res.-Atmos., 112, D03201, doi:10.1029/2006JD007436, 2007b.

Pope, C. A., Ezzati, M., and Dockery, D. W.: Fine-Particulate Air Pollution and Life Expectancy in the United States, New Engl. J. Med., 360, 376–386, doi:10.1056/NEJMsa0805646, 2009.

Presto, A. A. and Donahue, N. M.: Investigation of alpha-pinene plus ozone secondary organic aerosol formation at low total aerosol mass, Environ. Sci. Technol., 40, 3536–3543, doi:10.1021/es052203z, 2006.

Reardon, M. R., Allen, L., Bender, E. C., and Boyle, K. M.: Comparison of Motor Oils Using High-Temperature Gas Chromatography-Mass Spectrometry, J. Forensic Sci., 52, 656–663, doi:10.1111/j.1556-4029.2007.00421.x, 2007.

Robinson, A. L., Donahue, N. M., Shrivastava, M. K., Weitkamp, E. A., Sage, A. M., Grieshop, A. P., Lane, T. E., Pierce, J. R., and Pandis, S. N.: Rethinking organic aerosols: Semivolatile emissions and photochemical aging, Science, 315, 1259–1262, 2007.

Saleh, R., Shihadeh, A., and Khlystov, A.: On transport phenomena and equilibrium time scales in thermodenuders, Atmos. Meas. Tech. Discuss., 3, 2931–2960, doi:10.5194/amtd-3-2931-2010, 2010.

Shilling, J. E., Chen, Q., King, S. M., Rosenoern, T., Kroll, J. H., Worsnop, D. R., DeCarlo, P. F., Aiken, A. C., Sueper, D., Jimenez, J. L., and Martin, S. T.: Loading-dependent elemental composition of α-pinene SOA particles, Atmos. Chem. Phys., 9, 771–782, doi:10.5194/acp-9-771-2009, 2009.

Shu, J. N., Wilson, K. R., Ahmed, M., and Leone, S. R.: Coupling a versatile aerosol apparatus to a synchrotron: Vacuum ultraviolet light scattering, photoelectron imaging, and fragment free mass spectrometry, Rev. Sci. Instrum., 77, 043106,

doi:10.1063/1.2194474, 2006.

Smith, J. D., Kroll, J. H., Cappa, C. D., Che, D. L., Liu, C. L., Ahmed, M., Leone, S. R., Worsnop, D. R., and Wilson, K. R.: The heterogeneous reaction of hydroxyl radicals with submicron squalane particles: a model system for understanding the oxidative aging of ambient aerosols, Atmos. Chem. Phys., 9, 3209–3222, doi:10.5194/acp-9-3209-2009, 2009.

Tolocka, M. P., Heaton, K. J., Dreyfus, M. A., Wang, S., Zordan, C. A., Saul, T. D., and Johnston, M. V.: Chemistry of Particle Inception and Growth during α-Pinene Ozonolysis, Environ. Sci. Technol., 40, 1843–1848, doi:10.1021/es051926f, 2006.

Ulbrich, I., Lechner, M., and Jimenez, J. L., AMS Spectral Database, available at: http://cires.colorado.edu/jimenez-group/AMSsd/, 2010.

Ulbrich, I. M., Canagaratna, M. R., Zhang, Q., Worsnop, D. R., and Jimenez, J. L.: Interpretation of organic components from Positive Matrix Factorization of aerosol mass spectrometric data, Atmos. Chem. Phys., 9, 2891–2918, doi:10.5194/acp-9-2891-2009, 2009.

Vaden, T. D., Song, C., Zaveri, R. A., Imre, D., and Zelenyuk, A.: Morphology of mixed primary and secondary organic particles and the adsorption of spectator organic gases during aerosol formation, P. Natl. Acad. Sci. USA, 107, 6658–6663, doi:10.1073/pnas.0911206107, 2010.

Vaden, T. D., Imre, D., Beránek, J., Shrivastava, M. K., and Zelenyuk, A.: Evaporation kinetics and phase of laboratory and ambient secondary organic aerosol, P. Natl. Acad. Sci. USA, 108, 2190–2195, doi:10.1073/pnas.1013391108, 2011.

Virtanen, A., Joutsensaari, J., Koop, T., Kannosto, J., Yli-Pirila, P., Leskinen, J., Makela, J. M., Holopainen, J. K., Poschl, U., Kulmala, M., Worsnop, D. R., and Laaksonen, A.: An amorphous solid state of biogenic secondary organic aerosol particles, Nature, 467, 824–827, 2010.

Volkamer, R., Jimenez, J. L., San Martini, F., Dzepina, K., Zhang, Q., Salcedo, D., Molina, L. T., Worsnop, D. R., and Molina, M. J.: Secondary organic aerosol formation from anthropogenic air pollution: Rapid and higher than expected, Geophys. Res. Lett., 33, L17811, doi:10.1029/2006GL026899, 2006.

Yu, J. Z., Cocker, D. R., Griffin, R. J., Flagan, R. C., and Seinfeld, J. H.: Gas-phase ozone oxidation of monoterpenes: Gaseous and particulate products, J. Atmos. Chem., 34, 207–258, 1999.

Zahardis, J. and Petrucci, G. A.: The oleic acid-ozone heterogeneous reaction system: products, kinetics, secondary chemistry, and atmospheric implications of a model system – a review, Atmos. Chem. Phys., 7, 1237–1274, doi:10.5194/acp-7-1237-2007, 2007.

Zhang, Q., Jimenez, J. L., Canagaratna, M. R., Allan, J. D., Coe, H., Ulbrich, I., Alfarra, M. R., Takami, A., Middlebrook, A. M., Sun, Y. L., Dzepina, K., Dunlea, E., Docherty, K., DeCarlo, P. F., Salcedo, D., Onasch, T., Jayne, J. T., Miyoshi, T., Shimono, A., Hatakeyama, S., Takegawa, N., Kondo, Y., Schneider, J., Drewnick, F., Borrmann, S., Weimer, S., Demerjian, K., Williams, P., Bower, K., Bahreini, R., Cottrell, L., Griffin, R. J., Rautiainen, J., Sun, J. Y., Zhang, Y. M., and Worsnop, D. R.: Ubiquity and dominance of oxygenated species in organic aerosols in anthropogenically-influenced Northern Hemisphere midlatitudes, Geophys. Res. Lett., 34, L13801, doi:10.1029/2007GL029979, 2007.

Ziemann, P. J., Faulhaber, A. E., Huffman, J. A., Lechner,

M., and Jimenez, J. L., Combined Mass Spectra-Volatility Database, available at: http://cires.colorado.edu/jimenez-group/TDPBMSsd/, 2010.

Zobrist, B., Marcolli, C., Pedernera, D. A., and Koop, T.: Do atmospheric aerosols form glasses?, Atmos. Chem. Phys., 8, 5221–5244, doi:10.5194/acp-8-5221-2008, 2008.